Geophysical Research Letters

RESEARCH LETTER
10.1029/2025GL117094

Turbulent Aerosol Fluxes From Airborne Measurements Over the Arctic Ocean

David J. Simon[1], Jörg Hartmann[2], Jonas Schaefer[1], Sebastian Zeppenfeld[1], Christof Lüpkes[2], Markus Hartmann[1], Bruno Wetzel[1], Bernd Heinold[1], Zsófia Jurányi[2], Alexander Schulz[2], Laura Köhler[2], Anna-Marie Jörss[2], Andreas Herber[2], Silvia Henning[1], Mira L. Pöhlker[1], Gregory C. Roberts[3], and Frank Stratmann[1]

[1]Atmospheric Microphysics Department, Leibniz Institute for Tropospheric Research, Leipzig, Germany, [2]Alfred Wegener Institute, Helmholtz Centre for Polar and Marine Research, Bremerhaven, Germany, [3]Scripps Institution of Oceanography, La Jolla, CA, USA

Key Points:

- The novel platform T-Bird facilitates airborne studies on Arctic aerosol fluxes
- Fast size-resolved particle measurements are essential to characterize sea spray aerosol (SSA) fluxes in the marine boundary layer
- Our results suggest higher emissions in the accumulation mode size range than several sea salt source functions often used in climate models

Supporting Information:

Supporting Information may be found in the online version of this article.

Correspondence to:

D. J. Simon,
simon@tropos.de

Citation:

Simon, D. J., Hartmann, J., Schaefer, J., Zeppenfeld, S., Lüpkes, C., Hartmann, M., et al. (2025). Turbulent Aerosol fluxes from airborne measurements over the Arctic Ocean. *Geophysical Research Letters*, *52*, e2025GL117094. https://doi.org/10.1029/2025GL117094

Received 16 MAY 2025
Accepted 5 NOV 2025

Abstract Sea spray aerosol (SSA) emissions are an important source of natural aerosol particles, in particular over the remote Arctic Ocean. However, measurement data on SSA fluxes in the Arctic are sparse, such that these fluxes remain poorly constrained in atmospheric models. Utilizing simultaneous particle and turbulence measurements onboard the novel platform T-Bird, we quantitatively derive size-resolved SSA flux densities (dry diameter range 222–3,525 nm), representing the first airborne study on aerosol particle fluxes in the Arctic. In the accumulation mode size range, the measurements suggest roughly 100% higher emissions than predicted by commonly used sea salt generating functions. Our results constitute important information to evaluate model results, especially for the future Arctic, in which the magnitude of SSA fluxes is projected to increase as the sea ice retreats.

Plain Language Summary Aerosol particles emitted from the ocean to the atmosphere by wind-induced processes are an important component of the Arctic climate system. Quantifying these emissions is difficult such that corresponding data for the Arctic are sparse. We have successfully derived and quantified the rate of particle emission over the Arctic Ocean from airborne measurements for the first time. Our results may be used to assess the performance of atmospheric models in the Arctic, where more particles are expected to be emitted in the future as the sea ice melts due to global warming.

1. Introduction

Primary sea spray aerosol (SSA) production is a significant source of natural aerosol particles in marine environments, particularly in pristine locations such as over the Arctic Ocean (Willis et al., 2018). These SSA particles are emitted from the ocean to the atmosphere by wind-induced mechanisms and commonly comprise both organic matter and inorganic sea salt (De Leeuw et al., 2011). The mixing state between organics and inorganics and the size distribution of SSA affect, for example, the aerosol particles' optical properties as well as their ability to act as cloud condensation nuclei (CCN) (Ovadnevaite et al., 2011), and/or ice nucleating particles (INP) (DeMott et al., 2016). This carries significant implications concerning the Earth's radiative balance since SSA may directly interact with radiation by scattering and absorption processes, and indirectly (as CCN and INP) by mediating the formation, phase state, life time, and precipitation behavior of clouds (Andreae & Rosenfeld, 2008). Hence, SSA particles play a crucial role for aerosol-climate interactions in marine environments (Murphy et al., 1998; Pierce & Adams, 2006).

The Arctic is changing rapidly in response to climate change, a phenomenon commonly referred to as Arctic amplification (Serreze & Francis, 2006). One prominent manifestation of this process is the drastic decrease of sea ice (Stroeve et al., 2007), which entails dramatic consequences for the Arctic atmosphere (Wendisch et al., 2023). For example, the importance of SSA is expected to increase in the future Arctic as the sea ice retreats, resulting in expanding open water areas and thus increased SSA production (Browse et al., 2014; Gilgen et al., 2018; Struthers et al., 2011). Although studies widely agree that the emission of SSA will increase in the future, significant quantitative discrepancies between different modeling results exist, specifically with respect to the resulting radiative effects. Besides varying scenarios for the sea ice cover, these different outcomes largely result from uncertainties in the parametrization of SSA production fluxes and the SSA particle number size distribution (PNSD) (Lapere et al., 2023; Willis et al., 2018).

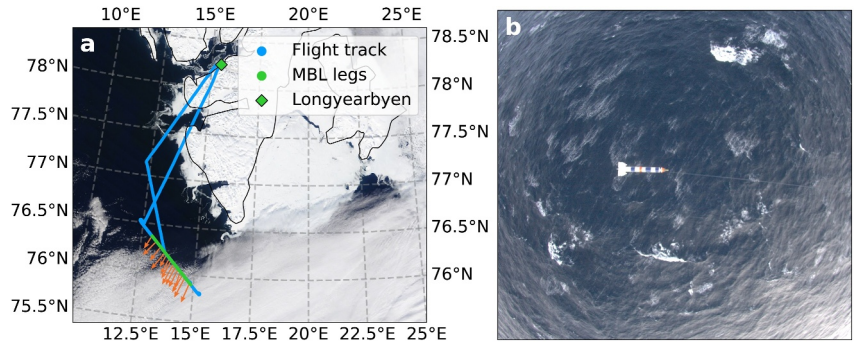

Figure 1. (a) Overview of the track of RF09. Several legs (cf. Figure 2) were flown in the same region such that the corresponding lines overlap. The green section highlights the legs inside the marine boundary layer considered in the further analysis (shaded areas in Figure 2). The arrows indicate the wind direction. The Moderate-resolution Imaging Spectroradiometer-TERRA satellite image was retrieved from https://wvs.earthdata.nasa.gov on 25 April 2024. (b) Fish-eye camera image facing downwards from the P6, taken during one of the low-level legs (11:17:27 UTC). The image shows the T-Bird as well as whitecaps on the sea surface.

Despite its importance, few in situ measurements of aerosol fluxes in the Arctic exist (Held et al., 2011; Markuszewski et al., 2024; Mathes et al., 2025; Nilsson et al., 2001). Mostly, eddy covariance systems have been used, set up at a fixed location on ice floes or ships. Such experiments are limited to the specific measurement location and influenced by the local environmental footprint (Buzorius et al., 2006). Moreover, flux measurements often employ condensation particle counters which do not provide any size-resolved information but can merely report integral particle number concentrations (Petroff et al., 2018). Aircraft measurements represent an alternative approach to stationary experiments, can inherently reach remote locations, and provide information on a regional scale (Buzorius et al., 2006). However, the lowermost part of the atmosphere remains inaccessible to aircraft, in particular during highly turbulent conditions. Here, towed-bodies such as the recently developed T-Bird (Jurányi et al., 2025) can extend the vertical sampling range and facilitate atmospheric measurements at low altitudes close to the surface, that is, the particle source in the case of SSA. To date solely two studies have utilized airborne platforms to determine aerosol fluxes (Buzorius et al., 2006; Lückerath et al., 2022), none of which in the Arctic.

Here, we report on aerosol fluxes derived from simultaneous particle and turbulence measurements at low altitudes over the open ocean onboard the T-Bird (T-Bird altitude $h_{\mathrm{Bird}} \approx 50$ m). To our knowledge, our study constitutes the first direct quantitative as well as size-resolved measurements of SSA fluxes from an airborne platform in the Arctic.

2. Methods

2.1. Campaign and Flight Overview

The airborne measurement campaign Boundary layer and Aerosol and Cloud Study in the Arctic, based on aircraft and T-Bird Measurements II took place from 5 April 2024 to 2 May 2024 and was based in Longyearbyen, Svalbard. Here, we focus on research flight 09 (RF09) on 25 April 2024 during which we encountered meteorological conditions with strong winds over the open ocean southwest of Svalbard (Figure 1a). Located in a region of pressure gradient between a high-pressure system to the north and a low-pressure system to the south, the target region was subject to strong easterly winds. In the northern sector, air masses from the ice-covered Storfjorden flowed over the Svalbard Mountains toward the Fram Strait (Figure S1 in Supporting Information S1, Kirbus & Wendisch, 2024; Spreen et al., 2008), where a marine boundary layer (MBL) developed, extending up to approximately 500 m above sea level (Figure S2 in Supporting Information S1), and resulting in sparse scattered cumuli clouds due to the foehn effect and mixing with warm and dry free tropospheric air. Further south, air masses from the sea ice flowed directly over the ocean south of Svalbard, resulting in increasing humidity, decreasing temperatures, and a lower cloud base with overcast conditions. The strong winds led to the formation of whitecaps on the sea surface (Figure 1b), indicative of breaking waves and bubble entrainment.

2.2. Measurement Instrumentation

2.2.1. T-Bird

The T-Bird is a towed-body system dragged by the research aircraft Polar 6 (P6) and was developed by the Alfred Wegener Institute, Helmholtz Center for Polar and Marine Research, with part of its aerosol payload as a contribution by the Leibniz-Institute for Tropospheric Research. It has been specifically designed to conduct simultaneous aerosol (Section 2.2.2) and turbulence measurements (Section 2.2.3) close to the surface (down to $h_{\mathrm{Bird,min}} \approx 10$ m, depending on the atmospheric conditions). The T-Bird is introduced in detail in Jurányi et al. (2025).

2.2.2. POPS

The Portable Optical Particle Spectrometer (POPS, Handix Scientific Inc., USA) is an optical particle counter, which sizes particles in a diameter range of approximately 140–3,300 nm based on their elastic light scattering intensity (Gao et al., 2016; Mei et al., 2020). POPS, which operates at a wavelength of 405 nm, measures the PNSDs at a high temporal resolution (1 Hz), and as a single-particle instrument is well suited for Arctic aerosol measurements (Pilz et al., 2022).

The diameter range reported above refers to the size of polystyrene latex spheres with which POPS is calibrated. We have converted the particle diameters based on the refractive index of dry sea salt particles (Text S4 in Supporting Information S1, Cotterell et al., 2017; Seinfeld & Pandis, 2006) and, throughout this paper, restrict our analysis to the range 222–3,525 nm.

2.2.3. Turbulence Measurements

An Aventech 5-hole-probe at the tip of the T-Bird is used for turbulence measurements. Pressure transducers are Setra 239 for alpha, beta and the dynamic pressure, and Setra 278 for the static pressure. Alpha and beta pressures are linked to the angles of attack and sideslip (see Hartmann et al., 2018). An open wire Pt100 in an unheated Rosemount housing is used for fast temperature measurements. These data are sampled at 100 Hz. Position and altitude are recorded by an iNAT-M200 that combines inertial measurements with a dual-antenna GNSS. GPS position is available at 1 Hz, inertial data is available up to 500 Hz. Data processing and system calibration is very similar to that used for the turbulence measurements of P6. See Hartmann et al. (2018) for further details.

3. Results and Discussion

3.1. Flight, Meteorology, and Aerosol Overview

The time series of the T-Bird's flight altitude is given in Figure 2a, together with the prevailing horizontal (b) and vertical wind speeds (c, both 100 Hz data). Figure 2b shows the air temperatures (100 Hz data) and, for the legs at low altitudes, sea surface temperatures (SSTs, 1 Hz data). Furthermore, POPS' measured particle number size distributions (d), and integral particle number concentrations (e, both 1 Hz data) in the size ranges 222–3,525 nm (N_{222}) and 396–3,525 nm (N_{396}) are depicted. In addition to the data at high temporal resolution, we show running means with a time window of $\Delta t = 30$ s in the subplots (b), (c), and (e).

We will focus our analysis on the flight sections highlighted by the shaded areas in Figure 2. These sections correspond to the flight leg outside of the MBL ("outside MBL", $h_{\mathrm{Bird}} \approx 1430$ m) and to those parts of the four low-level legs inside the MBL close to the sea surface ("inside MBL 1–4", $h_{\mathrm{Bird}} \approx 50$ m, cf. vertical profiles in Figure S2 in Supporting Information S1 regarding the stratification) which feature reasonably constant horizontal wind speeds and SSTs.

Throughout these parts of the MBL legs, which amount to a total measurement time of 3,587 s, both horizontal wind speeds and SSTs remained approximately constant at about 15 m s^{-1} and 4°C, respectively. The strong horizontal winds resulted in the presence of white caps (Figure 1b), and hence favorable conditions for SSA production (De Leeuw et al., 2011). This is supported by an elevated sodium concentration (540 ng m^{-3})—a conservative chemical tracer for SSA emissions (Barthel et al., 2019; White, 2008)—measured from an offline filter sampled at the T-Bird throughout all MBL legs. The concentration is consistent with typical atmospheric sodium levels in PM_{10} or $PM_{2.5}$ observed near the sea surface over a moderately rough, ice-free ocean (Kawana

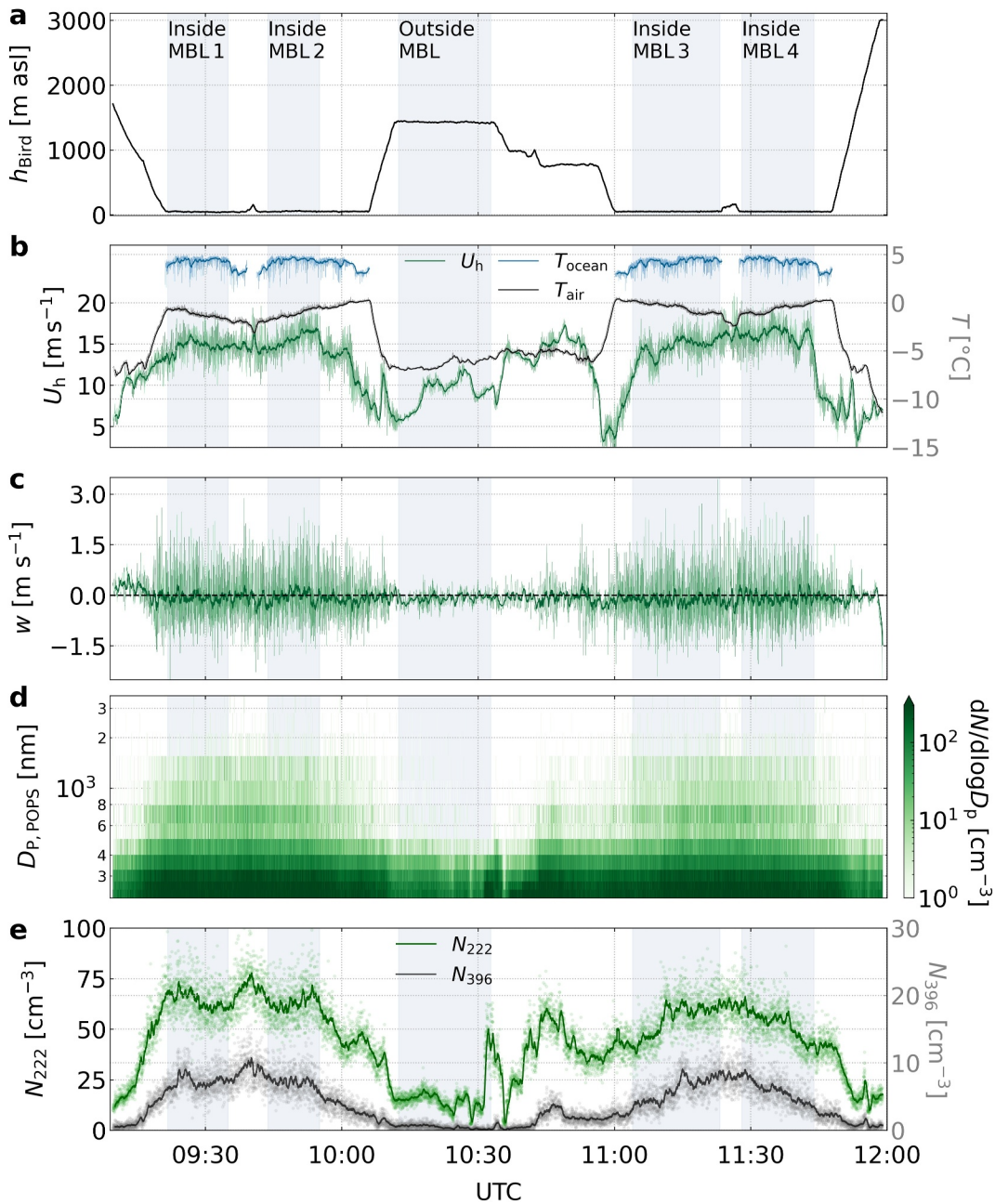

Figure 2. (a) Flight altitude above sea level of the T-Bird. (b) Horizontal wind speed (left *y*-axis), air temperature (right *y*-axis), and sea surface temperature (right *y*-axis). (c) Vertical wind speed. (d) Portable Optical Particle Spectrometer particle number size distribution. (e) Integral particle number concentrations N_{222} (left *y*-axis) and N_{396} (right *y*-axis). The shaded areas denote the flight sections considered in the analysis.

et al., 2021a, 2021b; Zeppenfeld et al., 2021, 2023) and much higher than measured at this day within the free troposphere onboard the P6 (Text S5 in Supporting Information S1, Grawe et al., 2023).

Strong fluctuations in vertical wind speeds inside the MBL can be seen in Figure 2c. Shear production dominated the turbulence near the surface, but buoyancy also contributed, as shown by a Monin-Obukhov length of −132 m at the measurement altitude (50 m). With respect to the encountered PNSDs, increased numbers of particles are found inside the boundary layer (Figure 2d). Integral particle number concentrations, N_{222} and N_{396} are shown as examples, were found to be significantly higher inside the MBL (Welch's *t*-test, $p < 0.0001$), with mean values of

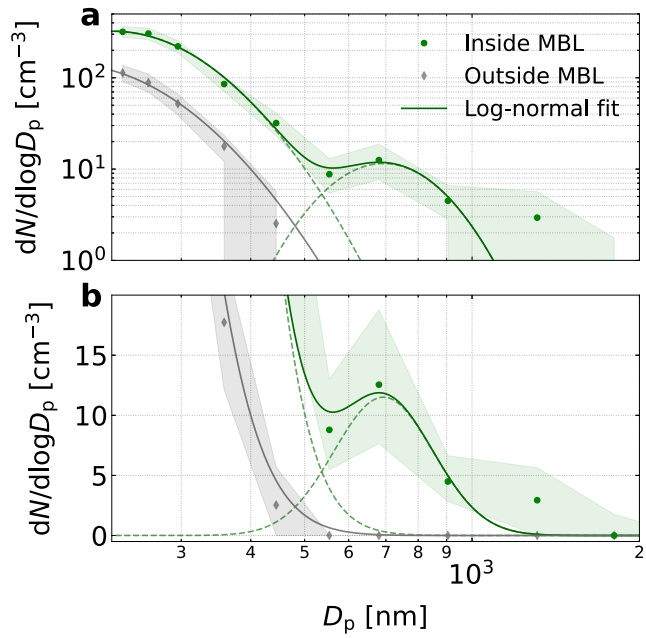

Figure 3. (a) Median particle number size distribution for the legs inside and outside of the marine boundary layer (MBL), fitted with log-normal distributions. The individual modes of the bi-modal distribution in the case of the MBL legs are shown as dashed lines. (b) The lower panel shows the same data as in (a) but on a linear ordinate and only up to a *y*-limit of 18 cm^{-3}.

$N_{222} \approx (58 \pm 11)$ cm^{-3} and $N_{396} \approx (6 \pm 2)$ cm^{-3} close to the sea surface, and $N_{222} \approx (16 \pm 9)$ cm^{-3} and $N_{396} \approx (0.5 \pm 0.4)$ cm^{-3} outside of the MBL (Figure 2e).

An increase of air temperature in horizontal direction from approximately - 2°C to 0°C was present in the region chosen for analysis (Figure 2b). Nevertheless, as wind is by far the dominant driver of SSA production (Lewis & Schwartz, 2004), we expect the variations in the PNSDs and particle fluxes due to the temperature gradient to be negligible. For example, Markuszewski et al. (2024) recently reported that the observed number flux densities in their large shipborne data set did not show significant correlations with air temperature over the Atlantic Ocean and merely a weak linear dependence over the Baltic Sea, while the particle flux densities depended exponentially on wind speed, with the latter in line with previous studies (e.g., Geever et al., 2005; Nilsson et al., 2001).

3.2. Particle Number Size Distribution

Figure 3 depicts the PNSD measured by POPS inside (green) and outside (gray) the MBL. The median distributions (markers) were calculated from the original PNSDs sampled at 1 Hz. The shaded areas correspond to the respective interquartile ranges. Additionally, fitted log-normal distributions are given (solid lines). For convenience, the size distributions are plotted on both a logarithmic (a) and linear (b) ordinate and shown only in the size range up to 2,000 nm as for larger diameters the number concentrations approach zero.

Comparing the size distributions measured in the MBL to those found aloft, it can be seen that in the boundary layer an additional mode in the size range above approximately 500 nm appeared (mean size around 690 nm). We interpret this as the sea salt mode, resulting from sea spray generation, in line with previous studies which reported mean dry diameters of the salt mode between about 500 and 750 nm from both in situ measurements and chamber experiments (Clarke et al., 2003; Heintzenberg et al., 2004; Salter et al., 2015; Zinke et al., 2022, 2024). In terms of number concentrations, this mode constitutes about 4.4% of the total aerosol particles in the size range between 222 and 3,525 nm, and 2.0% of the CCN measured at a supersaturation of $S = 0.2\%$ (Text S6 in Supporting Information S1, Roberts & Nenes, 2005). However, the sea salt mode accounts for 40.3% of the particle volume in this size range. In the size range below 500 nm, that is, in the accumulation mode size range, number concentrations were increased in the MBL as well. Following for example De Leeuw et al. (2011), this increase could result from small organic particles which are commonly emitted along with the salt particles. The hygroscopicity parameter of

$\kappa \approx 0.3$ found inside the MBL for accumulation mode particles points toward the respective direction (Text S6 in Supporting Information S1, Petters & Kreidenweis, 2007; Herenz et al., 2018; Pöhlker et al., 2023).

3.3. Turbulent Heat and Aerosol Flux Densities

3.3.1. Measured Flux Densities

Figure 4a shows the variance density spectra of vertical wind speed and temperature as a function of frequency ν. Indicative of the inertial subrange, both spectra follow a scaling of $\propto \nu^{-5/3}$ over two orders of magnitude. The Pearson correlation coefficient between w and T is clearly positive over the entire spectrum (Figure 4b, $p < 0.0001$) and lies in the typical range of a heat flux driven boundary layer (e.g., Arya, 2001). We can derive the turbulent sensible heat flux density by integrating the individual covariance density spectra (cf. Figure 4c) for each of the four MBL legs over ν, which yields a mean upward flux density of $F_{\text{heat}} \approx (99 \pm 7)\ \text{W m}^{-2}$. Corresponding mean environmental conditions for all flux densities derived in this section are $U_{\text{h}} = (15.2 \pm 1.7)\ \text{m s}^{-1}$, $T_{\text{air}} = (-0.8 \pm 0.5)$°C, and SST $= (4.3 \pm 0.5)$°C. The spectral analysis furthermore shows that eddies with a horizontal extent of about 300 m (flight altitude $h_{\text{Bird}} \approx 50$ m) contribute most to the vertical transport (vertical line denoted "scale" in Figure 4).

Before attempting to quantitatively calculate particle flux densities, we first evaluate the correlation between the vertical wind speed and the integral particle number concentrations N_{222}, N_{396}, N_{486}, N_{623}, and N_{744}. Larger particle sizes were not considered, as due to the low number concentrations, and the related low counting statistics, correlations between vertical wind speed and particle number concentration diminished. Generally, due to the inherently high noise level of the particle data, we cannot expect a similar level of correlation of particle number concentration with the vertical velocity as for temperature and vertical wind. Nevertheless, in all size ranges our data clearly show a positive correlation over the entire scale range available (Figure 4b). Considering a 5% significance level, all correlations were significant, except for N_{222} ($p \approx 0.3$). Interestingly, the correlation coefficient increases with particle size. We interpret this as a clear indication that these larger particles predominantly comprise freshly emitted SSA, while the total particle number concentration is influenced by background aerosol present in the lower size bins.

Similar to the calculation of the heat flux density, according to the eddy covariance method, we integrate the covariance density spectra (cf. Figure 4c, Text S7 in Supporting Information S1) and arrive at net particle flux densities of $F_{\text{N,222}} = (0.31 \pm 0.06) \times 10^6\ \text{m}^{-2}\ \text{s}^{-1}$, $F_{\text{N,396}} = (0.17 \pm 0.06) \times 10^6\ \text{m}^{-2}\ \text{s}^{-1}$, $F_{\text{N,486}} = (0.11 \pm 0.05) \times 10^6\ \text{m}^{-2}\ \text{s}^{-1}$, $F_{\text{N,623}} = (0.08 \pm 0.03) \times 10^6\ \text{m}^{-2}\ \text{s}^{-1}$, and $F_{\text{N,744}} = (0.05 \pm 0.02) \times 10^6\ \text{m}^{-2}\ \text{s}^{-1}$. The positive sign indicates upward fluxes, confirming that the ocean indeed acts as a source of aerosol particles in the MBL.

Note that we cannot resolve particle transport in the high-frequency range above the Nyquist frequency of POPS ($\nu_{\text{Ny}} = 1/(2\ \text{s})$, indicated by the line "2s" in Figure 4), and thus slightly underestimate the true flux densities. However, we clearly capture the dominant length scales of the turbulent particle transport ("scale" in Figure 4). To estimate the uncaptured particle flux density at high frequencies, we have integrated the well resolved heat flux density spectrum (a) up to the Nyquist frequency of the POPS data and (b) from that frequency up to the highest resolvable one (for the heat flux density). The former yields about 83% and the latter 17% of the total value. Assuming that the particle flux behaves similarly, we have increased the flux density values by 20% in Figure 4d. See Text S8 in Supporting Information S1 for further details on flux-related corrections and uncertainties (Ahlm et al., 2010; Buzorius et al., 2003; Coe & Gallagher, 1992; Horst, 1997; Lenschow & Raupach, 1991; Nilsson et al., 2021; Von der Weiden et al., 2009; Webb et al., 1980; Zinke et al., 2024).

Integral particle number concentrations measured by POPS partly deviated from those measured by a mobility particle size spectrometer (MPSS, Wiedensohler et al., 2018) operated onboard the P6. The discrepancies are small for particles in the sea salt size range but increase toward smaller diameters (Text S4 in Supporting Information S1). To account for these measurement uncertainties, we provide a range of flux densities in Figure 4d. The lower/upper values therein represent the lowest/highest values possible if we assume the POPS/MPSS measurements to correctly represent the true particle number concentrations.

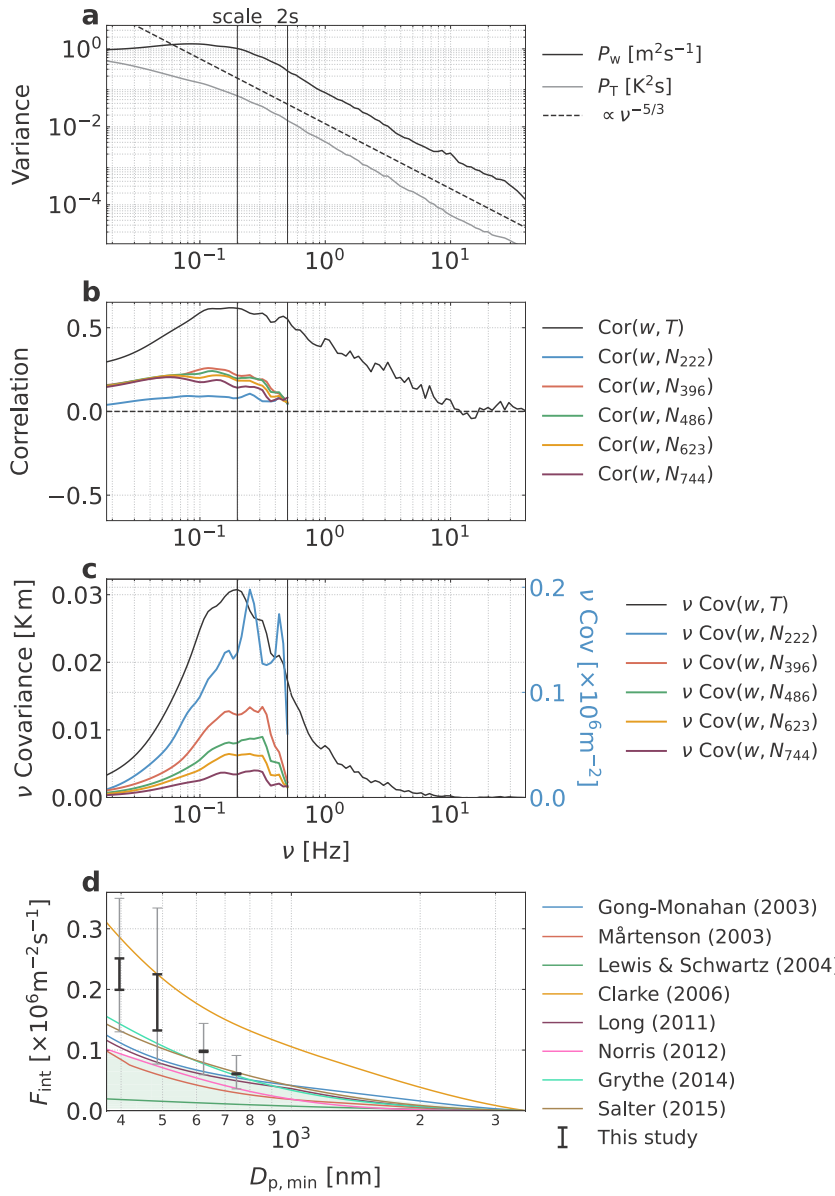

Figure 4. (a) Variance density spectrum of vertical wind speed and air temperature. The dashed line indicates the scaling in the inertial subrange. (b) Correlation coefficients between w and T, and w and $N_{222/396/486/623/744}$. (c) Covariance density spectrum of T and w (left y-axis), and w and $N_{222/396/486/623/744}$ (right y-axis), multiplied by frequency. The bold vertical lines show the Nyquist frequency of Portable Optical Particle Spectrometer (POPS) ($\nu_{Ny} = 1/(2\ s)$, "2s") and the frequency of the w-T-covariance spectrum's maximum, which corresponds to the length scale of maximum heat transport ("scale"). (d) Comparison of derived cumulative (integral) particle flux densities to sea salt generating functions. The black lines denote the range of mean values based on the POPS/MPSS-measured particle number concentrations, and the gray lines the corresponding standard deviations together with the uncertainty due to discrete particle counting. All data displayed in (a)–(d) represent the mean of the four marine boundary layer sections.

3.3.2. Discussion

Of the few studies on Arctic aerosol fluxes (Held et al., 2011; Markuszewski et al., 2024; Mathes et al., 2025; Nilsson et al., 2001), a comparison is only feasible in the case of Markuszewski et al. (2024), as the boundary conditions in the other studies differ significantly from those in this paper (Text S9 in Supporting Information S1). The measurements by Markuszewski et al. (2024) were conducted over open ocean for particles with dry diameters larger than approximately 250 nm, and flux densities were derived based on the gradient method. Using the given

function for a wind-dependent particle flux density, we obtain a value of $F_{N,Markuszewski} \approx 0.20 \times 10^6$ m^{-2} s^{-1}, similar to the result we have determined for $F_{N,396}$, that is, at somewhat larger diameters. Here, as well as in the subsequent paragraph, we have first converted the mean horizontal wind speed measured at $h_{Bird} \approx 50$ m to a reference height of 10 m using a logarithmic wind profile (Lewis & Schwartz, 2004).

Furthermore, we compare our results to various sea salt source functions commonly used in climate models (Grythe et al., 2014; Lapere et al., 2023). The functions tested include Monahan et al. (1986); Gong (2003); Mårtensson et al. (2003); Lewis and Schwartz (2004); Clarke et al. (2006); Long et al. (2011); Norris et al. (2012); Grythe et al. (2014); Salter et al. (2015). Because the source functions only consider salt emissions, except for Long et al. (2011) (Text S10 in Supporting Information S1), we refer to them as sea salt functions (in contrast to sea spray) and restrict the following discussion to the size range above 396 nm. Figure 4d depicts cumulative particle number flux densities, where we integrated the respective flux functions from 3,525 nm to 396 nm, since our measured flux densities also represent integral values in the ranges from 3,525 nm to 744/623/486/396 nm.

Our results lie at the upper end of the literature values, except for the formulation by Clarke et al. (2006), which predicts higher emissions over the entire size range. In the size ranges above 623 and 744 nm, which are dominated by sea salt, our results agree with several source functions, but differ when we include smaller particles in the calculations. The discrepancies might result from the increasing number of (non-sea salt) accumulation mode particles being present, which are not captured by the pure salt source functions. Another factor that might have contributed to the enhanced emissions is that the analyzed air mass spent relatively little time over the ocean (Figure S1 in Supporting Information S1), likely leading to low wave ages, which has been shown to be connected to increased SSA emissions (Markuszewski et al., 2024). Overall, our results exceed the emissions predicted by commonly used sea salt emission schemes by roughly 100% in the accumulation mode, and point toward the potentially important role of organics within accumulation mode sized sea spray particles. To further quantify the amount, composition, and emissions of such particles, additional measurements, in particular for smaller particle diameters and a larger range of wind speeds, are needed, and should be the objective of future studies.

4. Conclusion

In summary, using the towed-body T-Bird in the Arctic, we successfully carried out simultaneous turbulence and aerosol particle measurements. We derived, for the first time, SSA particle flux densities from airborne measurements at low altitudes ($h_{Bird} \approx 50$ m) over the ice-free Arctic Ocean. Our results highlight the importance of size-resolved investigations, and confirm the emissions produced by different sea salt source functions for particle sizes larger than 623 nm. For smaller particles, in particular in the accumulation mode size range (diameters smaller than about 500 nm), the measurements suggest higher emissions than predicted by several sea salt generating functions, likely due to the increased emission of organic material in that size range. Our results constitute important information to evaluate and/or drive current Arctic atmospheric models. Prospective studies could target the marginal sea ice zone, where aerosol particle fluxes are poorly characterized (Schmale et al., 2021), or other remote areas such as Antarctica. In the longer run, monitoring the changes of SSA fluxes expected in a changing climate can contribute to increasing the quality of future weather and climate models.

Conflict of Interest

The authors declare no conflicts of interest relevant to this study.

Data Availability Statement

The data used to derive the turbulent heat and particle fluxes in this study are available at PANGAEA via https://doi.org/10.1594/PANGAEA.976475 (turbulence data, Hartmann et al., 2025) and https://doi.org/10.1594/PANGAEA.976469 (particle data, Simon et al., 2025).

Acknowledgments
We gratefully acknowledge the funding by the Deutsche Forschungsgemeinschaft (DFG, German Research Foundation)—Project Number 268020496—TRR 172, within the framework of the Transregional Collaborative Research Center "ArctiC Amplification: Climate Relevant Atmospheric and SurfaCe Processes, and Feedback Mechanisms (AC)^3" and "TransArctic" (Project number 531020996). Open Access funding enabled and organized by Projekt DEAL.

References

Ahlm, L., Krejci, R., Nilsson, E. D., Mårtensson, E. M., Vogt, M., & Artaxo, P. (2010). Emission and dry deposition of accumulation mode particles in the Amazon basin. *Atmospheric Chemistry and Physics*, *10*(21), 10237–10253. https://doi.org/10.5194/acp-10-10237-2010

Andreae, M., & Rosenfeld, D. (2008). Aerosol–cloud–precipitation interactions. Part 1. The nature and sources of cloud-active aerosols. *Earth-Science Reviews*, *89*(1–2), 13–41. https://doi.org/10.1016/j.earscirev.2008.03.001

Arya, P. S. (2001). *Introduction to micrometeorology*. Elsevier.

Barthel, S., Tegen, I., & Wolke, R. (2019). Do new sea spray aerosol source functions improve the results of a regional aerosol model? *Atmospheric Environment*, *198*, 265–278. https://doi.org/10.1016/j.atmosenv.2018.10.016

Browse, J., Carslaw, K. S., Mann, G. W., Birch, C. E., Arnold, S. R., & Leck, C. (2014). The complex response of Arctic aerosol to sea-ice retreat. *Atmospheric Chemistry and Physics*, *14*(14), 7543–7557. https://doi.org/10.5194/acp-14-7543-2014

Buzorius, G., Kalogiros, J., & Varutbangkul, V. (2006). Airborne aerosol flux measurements with eddy correlation above the ocean in a coastal environment. *Journal of Aerosol Science*, *37*(10), 1267–1286. https://doi.org/10.1016/j.jaerosci.2005.11.006

Buzorius, G., Rannik, Ü., Nilsson, E., Vesala, T., & Kulmala, M. (2003). Analysis of measurement techniques to determine dry deposition velocities of aerosol particles with diameters less than 100 nm. *Journal of Aerosol Science*, *34*(6), 747–764. https://doi.org/10.1016/s0021-8502(03)00025-9

Clarke, A. D., Kapustin, V., Howell, S., Moore, K., Lienert, B., Masonis, S., et al. (2003). Sea-Salt size distributions from breaking waves: Implications for marine aerosol production and optical extinction measurements during SEAS. *Journal of Atmospheric and Oceanic Technology*, *20*(10), 1362–1374. https://doi.org/10.1175/1520-0426(2003)020⟨1362:SSDFBW⟩2.0.CO;2

Clarke, A. D., Owens, S. R., & Zhou, J. (2006). An ultrafine sea-salt flux from breaking waves: Implications for cloud condensation nuclei in the remote marine atmosphere. *Journal of Geophysical Research*, *111*(D6). https://doi.org/10.1029/2005JD006565

Coe, H., & Gallagher, M. (1992). Measurements of dry deposition of no2 to a dutch heathland using the eddy-correlation technique. *Quarterly Journal of the Royal Meteorological Society*, *118*(506), 767–786. https://doi.org/10.1002/qj.49711850608

Cotterell, M. I., Willoughby, R. E., Bzdek, B. R., Orr-Ewing, A. J., & Reid, J. P. (2017). A complete parameterisation of the relative humidity and wavelength dependence of the refractive index of hygroscopic inorganic aerosol particles. *Atmospheric Chemistry and Physics*, *17*(16), 9837–9851. https://doi.org/10.5194/acp-17-9837-2017

De Leeuw, G., Andreas, E. L., Anguelova, M. D., Fairall, C., Lewis, E. R., O'Dowd, C., et al. (2011). Production flux of sea spray aerosol. *Reviews of Geophysics*, *49*(2), RG2001. https://doi.org/10.1029/2010RG000349

DeMott, P. J., Hill, T. C., McCluskey, C. S., Prather, K. A., Collins, D. B., Sullivan, R. C., et al. (2016). Sea spray aerosol as a unique source of ice nucleating particles. *Proceedings of the National Academy of Sciences*, *113*(21), 5797–5803. https://doi.org/10.1073/pnas.1514034112

Gao, R., Telg, H., McLaughlin, R., Ciciora, S., Watts, L., Richardson, M., et al. (2016). A light-weight, high-sensitivity particle spectrometer for PM2.5 aerosol measurements. *Aerosol Science and Technology*, *50*(1), 88–99. https://doi.org/10.1080/02786826.2015.1131809

Geever, M., O'Dowd, C. D., van Ekeren, S., Flanagan, R., Nilsson, E. D., de Leeuw, G., & Rannik, Ü. (2005). Submicron sea spray fluxes. *Geophysical Research Letters*, *32*(15). https://doi.org/10.1029/2005GL023081

Gilgen, A., Huang, W. T. K., Ickes, L., Neubauer, D., & Lohmann, U. (2018). How important are future marine and shipping aerosol emissions in a warming Arctic summer and autumn? *Atmospheric Chemistry and Physics*, *18*(14), 10521–10555. https://doi.org/10.5194/acp-18-10521-2018

Gong, S. (2003). A parameterization of sea-salt aerosol source function for sub-and super-micron particles. *Global Biogeochemical Cycles*, *17*(4), 1097. https://doi.org/10.1029/2003GB002079

Grawe, S., Jentzsch, C., Schaefer, J., Wex, H., Mertes, S., & Stratmann, F. (2023). Next-generation ice-nucleating particle sampling on board aircraft: Characterization of the high-volume flow aerosol particle filter sampler (hera). *Atmospheric Measurement Techniques*, *16*(19), 4551–4570. https://doi.org/10.5194/amt-16-4551-2023

Grythe, H., Ström, J., Krejci, R., Quinn, P., & Stohl, A. (2014). A review of sea-spray aerosol source functions using a large global set of sea salt aerosol concentration measurements. *Atmospheric Chemistry and Physics*, *14*(3), 1277–1297. https://doi.org/10.5194/acp-14-1277-2014

Hartmann, J., Gehrmann, M., Kohnert, K., Metzger, S., & Sachs, T. (2018). New calibration procedures for airborne turbulence measurements and accuracy of the methane fluxes during the AirMeth campaigns. *Atmospheric Measurement Techniques*, *11*(7), 4567–4581. https://doi.org/10.5194/amt-11-4567-2018

Hartmann, J., Simon, D. J., & Schulz, A. (2025). High resolution airborne measurements of wind and temperature during the BACSAM II campaign in April 2024 [dataset]. *PANGAEA*. https://doi.org/10.1594/PANGAEA.976475

Heintzenberg, J., Birmili, W., Wiedensohler, A., Nowak, A., & Tuch, T. (2004). Structure, variability and persistence of the submicrometre marine aerosol. *Tellus B: Chemical and Physical Meteorology*, *56*(4), 357–367. https://doi.org/10.3402/tellusb.v56i4.16450

Held, A., Brooks, I. M., Leck, C., & Tjernström, M. (2011). On the potential contribution of open lead particle emissions to the central Arctic aerosol concentration. *Atmospheric Chemistry and Physics*, *11*(7), 3093–3105. https://doi.org/10.5194/acp-11-3093-2011

Herenz, P., Wex, H., Henning, S., Kristensen, T. B., Rubach, F., Roth, A., et al. (2018). Measurements of aerosol and CCN properties in the Mackenzie River delta (Canadian Arctic) during spring–summer transition in May 2014. *Atmospheric Chemistry and Physics*, *18*(7), 4477–4496. https://doi.org/10.5194/acp-18-4477-2018

Horst, T. (1997). A simple formula for attenuation of eddy fluxes measured with first-order-response scalar sensors. *Boundary-Layer Meteorology*, *82*(2), 219–233. https://doi.org/10.1023/A:1000229130034

Jurányi, Z., Lüpkes, C., Stratmann, F., Hartmann, J., Schaefer, J., Jörss, A.-M., et al. (2025). The t-bird – A new aircraft-towed instrument platform to measure aerosol properties and turbulence close to the surface: Introduction to the aerosol measurement system. *Atmospheric Measurement Techniques*, *18*(14), 3477–3494. https://doi.org/10.5194/amt-18-3477-2025

Kawana, K., Matsumoto, K., Taketani, F., Miyakawa, T., & Kanaya, Y. (2021a). Fluorescent biological aerosol particles over the central Pacific Ocean: Covariation with ocean surface biological activity indicators. *Atmospheric Chemistry and Physics*, *21*(20), 15969–15983. https://doi.org/10.5194/acp-21-15969-2021

Kawana, K., Matsumoto, K., Taketani, F., Miyakawa, T., & Kanaya, Y. (2021b). Chemical composition over the central Pacific Ocean in March 2019 [dataset]. PANGAEA. (In: Kawana, K et al. (2021): Distributions of Fluorescent bioaerosol particles and marine biological indicators over the central Pacific Ocean in March 2019 [dataset bundled publication]. PANGAEA, 10.1594/PANGAEA.936678). https://doi.org/10.1594/PANGAEA.936675

Kirbus, B., & Wendisch, M. (2024). Five-day backwards trajectories at one minute resolution along the flight tracks of the Polar 6 research aircraft during BACSAM II [dataset]. *PANGAEA*. https://doi.org/10.1594/PANGAEA.971694

Lapere, R., Thomas, J. L., Marelle, L., Ekman, A. M. L., Frey, M. M., Lund, M. T., et al. (2023). The representation of Sea salt aerosols and their role in polar climate within CMIP6. *Journal of Geophysical Research: Atmospheres*, *128*(6), e2022JD038235. https://doi.org/10.1029/2022JD038235

Lenschow, D., & Raupach, M. (1991). The attenuation of fluctuations in scalar concentrations through sampling tubes. *Journal of Geophysical Research*, *96*(D8), 15259–15268. https://doi.org/10.1029/91JD01437

Lewis, E. R., & Schwartz, S. E. (2004). Sea salt aerosol production: Mechanisms, methods, measurements and Models—A critical review. *Geophysical Monograph Series*, *152*, 3719. https://doi.org/10.1029/GM152

Long, M. S., Keene, W. C., Kieber, D., Erickson, D., & Maring, H. (2011). A sea-state based source function for size-and composition-resolved marine aerosol production. *Atmospheric Chemistry and Physics*, *11*(3), 1203–1216. https://doi.org/10.5194/acp-11-1203-2011

Lückerath, J., Held, A., Siebert, H., Michalkow, M., & Wehner, B. (2022). Vertical aerosol particle exchange in the marine boundary layer estimated from helicopter-borne measurements in the Azores region. *Atmospheric Chemistry and Physics*, *22*(15), 10007–10021. https://doi.org/10.5194/acp-22-10007-2022

Markuszewski, P., Nilsson, E. D., Zinke, J., Mårtensson, E. M., Salter, M., Makuch, P., et al. (2024). Multi-year gradient measurements of sea spray fluxes over the Baltic Sea and the North Atlantic Ocean. *Atmospheric Chemistry and Physics*, *24*(19), 11227–11253. https://doi.org/10.5194/acp-24-11227-2024

Mårtensson, E., Nilsson, E., de Leeuw, G., Cohen, L., & Hansson, H.-C. (2003). Laboratory simulations and parameterization of the primary marine aerosol production. *Journal of Geophysical Research*, *108*(D9), 4297. https://doi.org/10.1029/2002JD002263

Mathes, T., Guy, H., Prytherch, J., Kojoj, J., Brooks, I., Murto, S., et al. (2025). Particle flux-gradient relationships in the high Arctic: Emission and deposition patterns across three surface types. *Atmospheric Chemistry and Physics*, *25*(15), 8455–8474. https://doi.org/10.5194/acp-25-8455-2025

Mei, F., McMeeking, G., Pekour, M., Gao, R.-S., Kulkarni, G., China, S., et al. (2020). Performance assessment of Portable Optical Particle Spectrometer (POPS). *Sensors*, *20*(21), 6294. https://doi.org/10.3390/s20216294

Monahan, E. C., Spiel, D. E., & Davidson, K. L. (1986). A model of marine aerosol generation via whitecaps and wave disruption. In *Oceanic whitecaps: And their role in air-sea exchange processes* (pp. 167–174). Springer. https://doi.org/10.1007/978-94-009-4668-2_16

Murphy, D., Anderson, J., Quinn, P., McInnes, L., Brechtel, F., Kreidenweis, S., et al. (1998). Influence of sea-salt on aerosol radiative properties in the Southern Ocean marine boundary layer. *Nature*, *392*(6671), 62–65. https://doi.org/10.1038/32138

Nilsson, E., Hultin, K. A., Mårtensson, E. M., Markuszewski, P., Rosman, K., & Krejci, R. (2021). Baltic sea spray emissions: In situ eddy covariance fluxes vs. simulated tank sea spray. *Atmosphere*, *12*(2), 274. https://doi.org/10.3390/atmos12020274

Nilsson, E., Rannik, Ü., Swietlicki, E., Leck, C., Aalto, P. P., Zhou, J., & Norman, M. (2001). Turbulent aerosol fluxes over the Arctic Ocean: 2. Wind-driven sources from the sea. *Journal of Geophysical Research*, *106*(D23), 32139–32154. https://doi.org/10.1029/2000JD900747

Norris, S. J., Brooks, I. M., Hill, M. K., Brooks, B. J., Smith, M. H., & Sproson, D. A. (2012). Eddy covariance measurements of the sea spray aerosol flux over the open ocean. *Journal of Geophysical Research*, *117*(D7), D07210. https://doi.org/10.1029/2011JD016549

Ovadnevaite, J., Ceburnis, D., Martucci, G., Bialek, J., Monahan, C., Rinaldi, M., et al. (2011). Primary marine organic aerosol: A dichotomy of low hygroscopicity and high CCN activity. *Geophysical Research Letters*, *38*(21), L21806. https://doi.org/10.1029/2011GL048869

Petroff, A., Murphy, J., Thomas, S., & Geddes, J. A. (2018). Size-resolved aerosol fluxes above a temperate broadleaf forest. *Atmospheric Environment*, *190*, 359–375. https://doi.org/10.1016/j.atmosenv.2018.07.012

Petters, M. D., & Kreidenweis, S. M. (2007). A single parameter representation of hygroscopic growth and cloud condensation nucleus activity. *Atmospheric Chemistry and Physics*, *7*(8), 1961–1971. https://doi.org/10.5194/acp-7-1961-2007

Pierce, J. R., & Adams, P. J. (2006). Global evaluation of CCN formation by direct emission of sea salt and growth of ultrafine sea salt. *Journal of Geophysical Research*, *111*(D6), D06203. https://doi.org/10.1029/2005JD006186

Pilz, C., Düsing, S., Wehner, B., Müller, T., Siebert, H., Voigtländer, J., & Lonardi, M. (2022). CAMP: An instrumented platform for balloon-borne aerosol particle studies in the lower atmosphere. *Atmospheric Measurement Techniques*, *15*(23), 6889–6905. https://doi.org/10.5194/amt-15-6889-2022

Pöhlker, M. L., Pöhlker, C., Quaas, J., Mülmenstädt, J., Pozzer, A., Andreae, M. O., et al. (2023). Global organic and inorganic aerosol hygroscopicity and its effect on radiative forcing. *Nature Communications*, *14*(1), 6139. https://doi.org/10.1038/s41467-023-41695-8

Roberts, G. C., & Nenes, A. (2005). A continuous-flow streamwise thermal-gradient CCN chamber for atmospheric measurements. *Aerosol Science and Technology*, *39*(3), 206–221. https://doi.org/10.1080/027868290913988

Salter, M. E., Zieger, P., Acosta Navarro, J. C., Grythe, H., Kirkevåg, A., Rosati, B., et al. (2015). An empirically derived inorganic sea spray source function incorporating sea surface temperature. *Atmospheric Chemistry and Physics*, *15*(19), 11047–11066. https://doi.org/10.5194/acp-15-11047-2015

Schmale, J., Zieger, P., & Ekman, A. M. (2021). Aerosols in current and future Arctic climate. *Nature Climate Change*, *11*(2), 95–105. https://doi.org/10.1038/s41558-020-00969-5

Seinfeld, J. H., & Pandis, S. N. (2006). *Atmospheric chemistry and physics: From air pollution to climate change*. John Wiley and Sons.

Serreze, M. C., & Francis, J. A. (2006). The Arctic amplification debate. *Climatic Change*, *76*(3), 241–264. https://doi.org/10.1007/s10584-005-9017-y

Simon, D. J., Schaefer, J., Hartmann, M., Wetzel, B., & Stratmann, F. (2025). Size-resolved airborne in-situ measurements of aerosol particle number concentrations during the BACSAM II campaign in April 2024 [dataset]. *PANGAEA*. https://doi.org/10.1594/PANGAEA.976469

Spreen, G., Kaleschke, L., & Heygster, G. (2008). Sea ice remote sensing using AMSR-E 89-GHz channels. *Journal of Geophysical Research*, *113*(C2), C02S03. https://doi.org/10.1029/2005JC003384

Stroeve, J., Holland, M. M., Meier, W., Scambos, T., & Serreze, M. (2007). Arctic sea ice decline: Faster than forecast. *Geophysical Research Letters*, *34*(9), L09501. https://doi.org/10.1029/2007GL029703

Struthers, H., Ekman, A., Glantz, P., Iversen, T., Kirkevåg, A., Mårtensson, E. M., et al. (2011). The effect of sea ice loss on sea salt aerosol concentrations and the radiative balance in the Arctic. *Atmospheric Chemistry and Physics*, *11*(7), 3459–3477. https://doi.org/10.5194/acp-11-3459-2011

Von der Weiden, S.-L., Drewnick, F., & Borrmann, S. (2009). Particle loss calculator–a new software tool for the assessment of the performance of aerosol inlet systems. *Atmospheric Measurement Techniques*, *2*(2), 479–494. https://doi.org/10.5194/amt-2-479-2009

Webb, E. K., Pearman, G. I., & Leuning, R. (1980). Correction of flux measurements for density effects due to heat and water vapour transfer. *Quarterly Journal of the Royal Meteorological Society*, *106*(447), 85–100. https://doi.org/10.1002/qj.49710644707

Wendisch, M., Brückner, M., Crewell, S., Ehrlich, A., Notholt, J., Lüpkes, C., et al. (2023). Atmospheric and surface processes, and feedback mechanisms determining Arctic amplification: A review of first results and prospects of the (AC)3 project. *Bulletin of the American Meteorological Society*, *104*(1), E208–E242. https://doi.org/10.1175/bams-d-21-0218.1

White, W. H. (2008). Chemical markers for sea salt in improve aerosol data. *Atmospheric Environment*, *42*(2), 261–274. https://doi.org/10.1016/j.atmosenv.2007.09.040

Wiedensohler, A., Wiesner, A., Weinhold, K., Birmili, W., Hermann, M., Merkel, M., et al. (2018). Mobility particle size spectrometers: Calibration procedures and measurement uncertainties. *Aerosol Science and Technology*, *52*(2), 146–164. https://doi.org/10.1080/02786826.2017.1387229

Willis, M. D., Leaitch, W. R., & Abbatt, J. P. (2018). Processes controlling the composition and abundance of Arctic aerosol. *Reviews of Geophysics*, *56*(4), 621–671. https://doi.org/10.1029/2018RG000602

Zeppenfeld, S., van Pinxteren, M., Hartmann, M., Zeising, M., Bracher, A., & Herrmann, H. (2023). Marine carbohydrates in arctic aerosol particles and fog – Diversity of oceanic sources and atmospheric transformations. *Atmospheric Chemistry and Physics*, *23*(24), 15561–15587. https://doi.org/10.5194/acp-23-15561-2023

Zeppenfeld, S., van Pinxteren, M., van Pinxteren, D., Wex, H., Berdalet, E., Vaqué, D., et al. (2021). Aerosol marine primary carbohydrates and atmospheric transformation in the western antarctic peninsula. *ACS Earth and Space Chemistry*, *5*(5), 1032–1047. https://doi.org/10.1021/acsearthspacechem.0c00351

Zinke, J., Nilsson, E. D., Markuszewski, P., Zieger, P., Mårtensson, E. M., Rutgersson, A., & Salter, M. E. (2024). Sea spray emissions from the Baltic Sea: Comparison of aerosol eddy covariance fluxes and chamber-simulated sea spray emissions. *Atmospheric Chemistry and Physics*, *24*(3), 1895–1918. https://doi.org/10.5194/acp-24-1895-2024

Zinke, J., Nilsson, E. D., Zieger, P., & Salter, M. E. (2022). The effect of seawater salinity and seawater temperature on sea salt aerosol production. *Journal of Geophysical Research: Atmospheres*, *127*(16), e2021JD036005. https://doi.org/10.1029/2021JD036005